Inorganic Chemistry

Article

pubs.acs.org/IC

Protonation Studies of a Mono-Dinitrogen Complex of Chromium Supported by a 12-Membered Phosphorus Macrocycle Containing Pendant Amines

Michael T. Mock,*[,‡] Aaron W. Pierpont,[‡] Jonathan D. Egbert,[‡] Molly O'Hagan,[‡] Shentan Chen,[‡] R. Morris Bullock,[‡] William G. Dougherty,[†] W. Scott Kassel,[†] and Roger Rousseau[‡]

[‡]Center for Molecular Electrocatalysis, Physical Sciences Division, Pacific Northwest National Laboratory, Richland, Washington 99352, United States

[†]Department of Chemistry, Villanova University, Villanova, Pennsylvania 19085, United States

Supporting Information

ABSTRACT: The reduction of *fac*-[$CrCl_3(P^{Ph}{}_3N^{Bn}{}_3)$], (**1-($Cl_3$)**), ($P^{Ph}{}_3N^{Bn}{}_3$ = 1,5,9-tribenzyl-3,7,11-triphenyl-1,5,9-triaza-3,7,11-triphosphacyclododecane) with Mg in the presence of dmpe (dmpe = 1,2-bis(dimethylphosphino)ethane) affords the first example of a monodinitrogen Cr^0 complex, $Cr(N_2)$-(dmpe)($P^{Ph}{}_3N^{Bn}{}_3$), (**2(N_2)**), containing a pentaphosphine coordination environment. **2(N_2)** is supported by a unique facially coordinating 12-membered phosphorus macrocycle containing pendant amine groups in the second coordination sphere. Treatment of **2(N_2)** at −78 °C with 1 equiv of $[H(OEt_2)_2][B(C_6F_5)_4]$ results in protonation of the metal center, generating the seven-coordinate Cr^{II}−N_2 hydride complex, $[Cr(H)(N_2)(dmpe)(P^{Ph}{}_3N^{Bn}{}_3)][B(C_6F_5)_4]$, [**2(H)($N_2$)**]$^+$. Treatment of **2($^{15}N_2$)** with excess triflic acid at −50 °C afforded a trace amount of $^{15}NH_4{}^+$ from the reduction of the coordinated $^{15}N_2$ ligand (electrons originate from Cr). Electronic structure calculations were employed to evaluate the pK_a values of three protonated sites of **2(N_2)** (metal center, pendant amine, and N_2 ligand) and were used to predict the thermodynamically preferred Cr-N_xH_y intermediates in the N_2 reduction pathway for **2(N_2)** and the recently published complex *trans*-$[Cr(N_2)_2(P^{Ph}{}_4N^{Bn}{}_4)]$ upon the addition of protons and electrons.

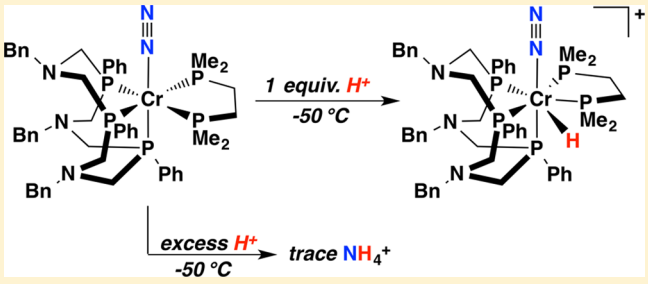

INTRODUCTION

The synthesis and reactivity of transition metal dinitrogen complexes continue to be a heavily explored area of research, especially in the design of molecular systems that further the understanding of N_2 reduction to form ammonia in biological (nitrogenase enzyme)[1] and heterogeneous (Haber−Bosch process)[2] systems. In particular, low-valent molybdenum and tungsten bis(dinitrogen) complexes containing phosphine ligands, i.e., $M(N_2)_2(P)_4$ and $M(N_2)_2(P\text{-}P)_2$, (M = Mo or W; P = monodentate phosphine, P-P = bidentate phosphine), represent an extensively studied structure type.[3] The identification of molybdenum in the active site of nitrogenase inspired early work with these molecules aimed at elucidating mechanistic details of N_2 reduction. Accordingly, identification of protonated N_2 intermediates, such as the hydrazido (Mo-NNH_2) species, and the stoichiometric formation of ammonia by a homogeneous molybdenum containing system symbolized significant early discoveries.[3−5]

The utilization of tridentate phosphine ligands was shown to enhance the stability of the complexes, especially upon oxidation of the Mo center. George and co-workers thoroughly explored the reactivity of monodinitrogen complexes of the type $Mo(N_2)$(triphos)(P-P) (triphos = $(PhP(CH_2CH_2PPh_2)_2)$, which contained tridentate and bidentate phosphine ligands.[6,7] Much like their bis(dinitrogen) counterparts, treatment with mineral acids yielded ammonia and hydrazine.[8] More recently, Tuczek and co-workers have prepared a variety of low-valent molybdenum mono- and bis(dinitrogen) complexes bearing tridentate and tetradentate phosphine ligands.[9] In particular, recent studies reported a family of molybdenum monodinitrogen complexes bearing facially capping tripodal phosphine ligands and a chelating diphosphine ligand.[10] These new ligand designs are intended to more effectively modulate the steric and electronic environment about the N_2 ligand, in addition to affording more robust Mo-N_2 complexes that are less prone to ligand loss. Indeed, the complexes that catalyze the reduction of N_2 to NH_3 from the groups of Schrock,[11] Nishibayashi,[12] and Peters[13] utilize multidentate ligand platforms.

While numerous examples of low-valent molybdenum dinitrogen complexes with monodentate, bidentate, and tridentate phosphine ligands have been prepared, comparatively few dinitrogen complexes of the first row congener, Cr, have been reported. The scarcity of these complexes is presumably a

Received: February 12, 2015
Published: May 1, 2015

DOI: 10.1021/acs.inorgchem.5b00351
Inorg. Chem. 2015, 54, 4827−4839

reflection of weak N_2 binding to Cr.[14] Contrary to this assessment, our group has prepared stable Cr-dinitrogen complexes supported by phosphine ligand scaffolds that contain pendant amine groups in the second coordination sphere such as the cyclic [8]-$P^R_2N^{R'}_2$ ligands ($P^R_2N^{R'}_2$ = 1,5-diaza-3,7-diphosphacyclooctanes) in the complex *cis*-$[Cr(N_2)_2(P^{Ph}_2N^{Bn}_2)_2]$, (Ph = phenyl; Bn = benzyl).[15] Recently, we reported the formation of 12-membered ([12]-$P^{Ph}_3N^{Bn}_3$) and 16-membered ([16]-$P^{Ph}_4N^{Bn}_4$) phosphorus macrocycles resulting from an unexpected ring expansion of the [8]-$P^{Ph}_2N^{Bn}_2$ ligand. The $P^{Ph}_4N^{Bn}_4$ ligand was utilized to prepare the Cr bis(dinitrogen) complex, *trans*-$[Cr(N_2)_2(P^{Ph}_4N^{Bn}_4)]$ ($P^{Ph}_4N^{Bn}_4$ = 1,5,9,13-tetrabenzyl-3,7,11,15-tetraphenyl-1,5,9,13-tetraaza-3,7,11,15-tetraphosphacyclohexadecane), and subsequent reactivity with HOTf afforded the preferential formation of hydrazine from reduction of the N_2 ligands. Building on these encouraging results, we sought to utilize the smaller [12]-$P^{Ph}_3N^{Bn}_3$ macrocycle to prepare a Cr-dinitrogen complex. Herein we describe the preparation, characterization, and acid reactivity of the first mono-dinitrogen complex of Cr in a pentaphosphine coordination environment. In addition, we present computational results that examine the thermodynamically preferred N_2 reduction pathways resulting from the addition of protons and electrons to Cr-N_2 complexes bearing the $P^{Ph}_3N^{Bn}_3$ and $P^{Ph}_4N^{Bn}_4$ ligands in order to rationalize differences in their reactivity profiles.

RESULTS AND DISCUSSION

Synthesis and Characterization of $Cr(N_2)$(dmpe)-($P^{Ph}_3N^{Bn}_3$), $2(N_2)$. As described in our earlier report, the facially coordinating 12-membered phosphorus macrocycle, [12]-$P^{Ph}_3N^{Bn}_3$, is generated by stirring $CrCl_2(THF)$ and $P^{Ph}_2N^{Bn}_2$ in THF. The ligand is isolated as the Cr^{III} complex, *fac*-$[CrCl_3(P^{Ph}_3N^{Bn}_3)]$ ($\mathbf{1(Cl_3)}$), a blue crystalline solid in 25% yield.[16] To synthesize a mono-dinitrogen Cr complex consisting of a coordination sphere of five phosphorus donors, diphosphine ligands were selected that contain electron-donating alkyl substituents in order to produce an electron-rich Cr center to activate the coordinated N_2 ligand.[10b] In addition, diphosphine ligands with a small steric profile were selected in an effort to avoid impeding coordination to the metal. Accordingly, dmpm (dmpm = $(CH_3)_2PCH_2P(CH_3)_2$) and dmpe were investigated as coligands that satisfied these requirements. A blue suspension of $\mathbf{1(Cl_3)}$ and 1 equiv of the diphosphine ligand was stirred in THF with excess Mg powder under an N_2 atmosphere for ca. 24−36 h, according to eq 1.

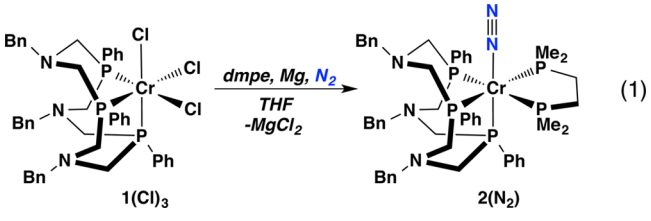

(1)

Reactions employing dmpe afforded the mono-dinitrogen complex $Cr(N_2)$(dmpe)($P^{Ph}_3N^{Bn}_3$) ($\mathbf{2(N_2)}$) as dark red crystals in 80% yield. Careful addition of only 1 equiv of dmpe is necessary to preclude the formation of *trans*-$[Cr(N_2)_2(dmpe)_2]$.[17] Complex $\mathbf{2(N_2)}$ is stable at room temperature as a solid, or in THF, diethyl ether, or pentane solutions for weeks under an N_2 atmosphere. In contrast to dmpe, when dmpm was employed as a ligand during the reduction of $\mathbf{1(Cl_3)}$, a dinitrogen complex could not be identified. While this result was surprising, it is reasonable to propose that the larger bite angle from the two-carbon backbone of dmpe is necessary to form the octahedral complex, as the inability to form the product with dmpm due to steric reasons is not expected to occur.

The molecular structure of $\mathbf{2(N_2)}$ is shown in Figure 1. The Cr^0 center exhibits a slightly distorted octahedral geometry in

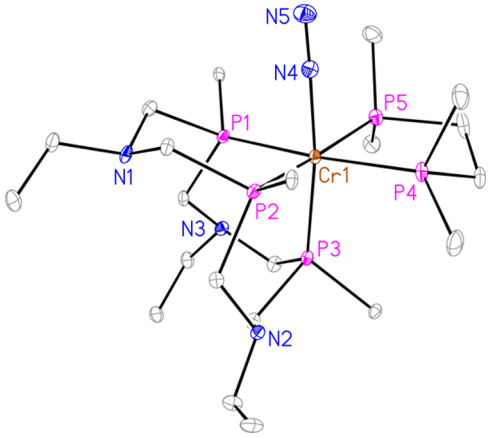

Figure 1. Molecular structure of $Cr(N_2)$(dmpe)($P^{Ph}_3N^{Bn}_3$) ($\mathbf{2(N_2)}$). Only *ipso* carbons of the phenyl groups bound to phosphorus and methylene and *ipso* carbons of the benzyl groups are shown. Thermal ellipsoids are drawn at 30% probability. Hydrogen atoms are omitted. Selected bond distances (Å) and angles (deg): Cr−N4 = 1.873(3), Cr−P1 = 2.2591(8), Cr−P2 = 2.2834(9), Cr−P3 = 2.3163(9), Cr−P4 = 2.3342(9), Cr−P5 = 2.3150(9), N4−N5 = 1.132(3), P1−Cr−P2 = 89.54(3), P2−Cr−P3 = 90.08(3), P1−Cr−P3 = 86.46(3), P4−Cr−P5 = 81.21(3), P3−Cr−N4 = 172.63(8), Cr−N4−N5 = 177.7(3).

which of two phosphorus atoms (P1 and P2) of the [12]-$P^{Ph}_3N^{Bn}_3$ ligand, and two phosphorus atoms (P4 and P5) of dmpe occupy the equatorial sites of the complex. The third phosphorus atom (P3) of the [12]-$P^{Ph}_3N^{Bn}_3$ ligand and the end-on bound dinitrogen ligand occupy the axial positions. The P−Cr−P bond angles of the [12]-$P^{Ph}_3N^{Bn}_3$ ligand range from 86.5−90.1°, reflecting an ideal ring size to coordinate as a facially capping ligand. In the solid state, two of the benzylamine groups are pointed toward the Cr center, while the third benzylamine group (N1), which is also closest to the N_2 ligand, is pointed away from Cr and consequently directed away from the bound N_2 ligand. We observed an analogous orientation of the pendant amine lone pair (closest to the N_2 ligand) in the solid-state structure of *cis*-$[Cr(N_2)_2(P^{Ph}_2N^{Bn}_2)_2]$ in which the four six-membered rings are in the chair conformation, decreasing the steric interactions between benzyl groups, but also minimizing electrostatic interactions between the electron lone pairs on the amine and the terminal nitrogen atom of the N_2 ligands.[15] The P_3 ring conformation in $\mathbf{1(Cl_3)}$[16] and in other facially coordinating 12-membered P_3 macrocycles that are bound to MX_3 fragments (M = Cr,[18] Mo; X = Cl, CO) and contain methylene groups in the ligand backbone, such as 1,5,9-triphosphacyclododecane or analogues with alkyl[19] or aryl[20] functionalized phosphines, typically adopt a "crown" or "partial crown"[21] geometry in which the central atom of the three atom backbone is pointed inward toward the center of the macrocycle. The additional steric bulk of the benzylamine groups and steric effects from the methyl groups of the dmpe

DOI: 10.1021/acs.inorgchem.5b00351
Inorg. Chem. 2015, 54, 4827−4839

Table 1. Infrared, Crystallographic, and ^{15}N NMR Spectroscopic Data for Selected Dinitrogen Complexes of Cr, Mo, and W

	ν_{NN} (cm^{-1})[a]	N–N (Å)	δ ^{15}N NMR (ppm)[b]	ref
$Cr(N_2)(dmpe)(P^{Ph}{}_3N^{Bn}{}_3)$ **2(N$_2$)**	1918[c]	1.132(3)	−10.3, −14.5 (J_{NN} = 7)[c]	this work
cis-$[Cr(N_2)_2(P^{Ph}{}_2N^{Bn}{}_2)_2]$	2009, 1937[c]	1.133(3)	−2.4 (J_{NN} = 6), −13.4[c]	15
trans-$[Cr(N_2)_2(P^{Ph}{}_4N^{Bn}{}_4)]$	2072, 1918[c]	1.112(3) 1.120(3)	−27.0; −34.6, −38.9[c]	16
trans-$[Cr(N_2)_2(dmpe)_2]$	1932[d]	1.122(3)	−26.5, −37.8 (J_{NN} = 6)[c]	17b
cis-$[Cr(N_2)_2(PMe_3)_4]$	1990, 1918[e]			24
trans-$[Mo(N_2)_2(depe)_2]$	1921[f]	1.117(7)	−42.0, −43.4 (J_{NN} = 5.7)[c]	25–27
$Mo(N_2)$(tdppme)(dmpm)	1979[f]	1.069(8)	−25.6 (J_{NN} = 5.7), −33.3[h]	28
$Mo(N_2)$(dpepp)(depe)	1952[f]			29
$Mo(N_2)$(trpd-1)(dmpm)	1965[f]	1.055(3)		10a
$Mo(N_2)$(dpepp)(dppm)	1979[f]	1.119(8)	−30.5, −15.7 (J_{NN} = 5.7)[c]	30
$Mo(N_2)(SiP_3)$(dmpm)	1943[g]			10b
$Mo(N_2)(SiP^{Me}{}_2P^{iPr})$(dmpm)	1932[g]			10c
cis-$[Mo(N_2)_2(PMe_3)_4]$	2010, 1965[d]	1.15(1) 1.14(1)		31
$Mo(N_2)(PMe_3)_5$	1950[d]	1.12(3)		32, 31
cis-$[W(N_2)_2(PMe_2Ph)_4]$	1998, 1931[h]	1.125(4) 1.120(4)	−57.8, −32.5 (J_{NN} = 6)[c]	33, 27
trans-$[W(N_2)_2(PPh_2Me)_4]$	1900, 1973[f]	1.134(2) 1.132(2)		34, 35
trans-$[W(N_2)_2(dppe)_2]$	1943, 2008[f]	1.126(15) 1.141(16)	−60.1, −48.6 (J_{NN} = 5)[c]	36, 27, 35
trans-$[W(N_2)_2(depe)_2]$	1891[e]		−63.7, −52.4 (J_{NN} = 6)[c]	26, 27
cis-$[W(N_2)_2(PMe_3)_4]$	1980, 1920[d]			37
$W(N_2)(PMe_3)_5$	1905[d]	1.11(2)		37

[a]For $^{14}N_2$. [b]Referenced to CH_3NO_2 at 0 ppm. [c]Recorded in THF. [d]hexane. [e]Nujol. [f]KBr. [g]ATR. [h]Benzene, trpd-1 = $MeC(CH_2PPh_2)_2(CH_2P^iPr_2)$, tdppme = 1,1,1-tris(diphenylphosphinomethyl)ethane, dpepp = bis(diphenylphosphinoethyl)phenylphosphine

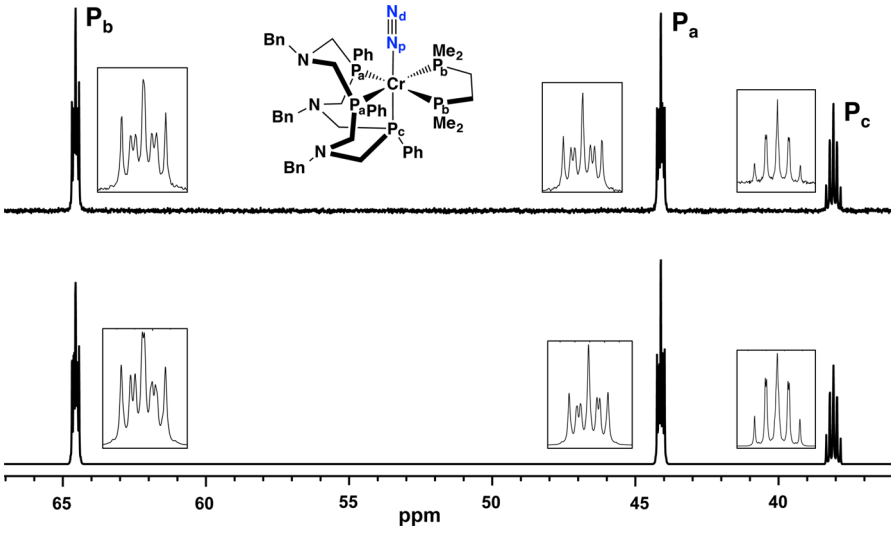

Figure 2. Measured (top) and simulated (bottom) $^{31}P\{^1H\}$ NMR spectra of **2(N$_2$)** recorded at 21 °C in THF-d_8.

ligand in **2(N$_2$)** may contribute to the positioning of the amine nitrogen atoms in the [12]-$P^{Ph}{}_3N^{Bn}{}_3$ described above. The P4–Cr1–P5 bond angle of the dmpe ligand is 81.21(3)°, smaller than in the P_3 macrocycle. The Cr–P bond lengths to the [12]-$P^{Ph}{}_3N^{Bn}{}_3$ ligand are in the range of 2.259–2.316 Å, with the Cr1–P3 (positioned trans to N_2) being the longest. Metric parameters about the dinitrogen ligand include the Cr–N4 bond length of 1.873(3) Å, and the N≡N triple bond (N4–N5) of 1.132(3) Å.

The IR spectrum corroborates the modest degree of activation for the end-on bound N_2 ligand with an ν_{NN} band at 1918 cm^{-1} in THF (1912 cm^{-1} KBr). Validating this assignment, the ν_{NN} band appears at 1855 cm^{-1} in THF for a sample prepared with $^{15}N_2$ gas, $Cr(^{15}N_2)(dmpe)(P^{Ph}{}_3N^{Bn}{}_3)$ **2(^{15}N$_2$)**. The N_2 vibrational frequency in **2(N$_2$)** is noteworthy and suggests the end-on N_2 ligand is activated to a greater extent compared to similar Mo mono-dinitrogen complexes with a pentaphosphine coordination environment, including complexes containing *only* electron-donating alkylphosphine groups. For example, the mono-dinitrogen complexes $Mo(N_2)(SiP_3)$(dmpm)[10b] and $Mo(N_2)(SiP^{Me}{}_2P^{iPr})$(dmpm)[10c] reported by Tuczek and co-workers, containing dmpm and a facially coordinating tripodal phosphine ligand bearing methyl or isopropyl substituents (SiP_3 = tris(dimethylphosphinomethyl)-methylsilane; $SiP^{Me}{}_2P^{iPr}$ = [(diisopropylphosphino)methyl]-bis[(dimethylphosphino)methyl](methylsilane)) exhibit N_2 vibrational frequencies of 1943 and 1932 cm^{-1}, respectively. The N_2 vibrational frequency in **2(N$_2$)** that is 14–25 cm^{-1} lower in energy is striking considering two factors: (1) the [12]-$P^{Ph}{}_3N^{Bn}{}_3$ ligand contains electron-withdrawing phenyl substituents on the phosphorus atoms and (2) a periodic dependence on the activation of N_2 is expected; that is, a lower N_2 vibrational frequency for coordinated N_2 ligands is anticipated upon descending the group 6 metals, W > Mo >

DOI: 10.1021/acs.inorgchem.5b00351
Inorg. Chem. 2015, 54, 4827–4839

Cr due to the more diffuse nature of the metal d-orbitals, increasing electron density into π^* orbitals of the N_2 ligand.[22] Notably, Tuczek and co-workers recently reported the in situ formation of two Mo mono-dinitrogen complexes bearing a mixed phosphine/N-heterocyclic carbene ligand, *mer*-[Mo(N_2)(PCP)(PPh_2Me)$_2$] and *fac*-[Mo(N_2)(PCP)(dmpm)] (PCP = 1,3-bis(2-diphenylphosphanyl-ethyl)imidazole-2-ylidene) which exhibit ν_{NN} bands at 1876 and 1881 cm^{-1}, respectively, reflecting the effect of the strong σ-donating carbene group trans disposed to the N_2 ligand.[23] Table 1 contains infrared, crystallographic, and ^{15}N NMR spectroscopic data, for selected Cr, Mo, and W-N_2 complexes, including group 6 complexes with pentaphosphine coordination environments. From this data it can be concluded that **2(N$_2$)** exhibits one of the most activated N≡N bonds of a terminally bound N_2 ligand in the Cr-based systems, based on the low value of the ν_{NN} band. The extent of N_2 activation in **2(N$_2$)** is greater than many Mo and W-N_2 complexes, which are known to produce hydrazine and/or ammonia upon the addition of strong acids.

The $^{31}P\{^1H\}$ NMR spectrum of **2(N$_2$)** recorded at 21 °C in THF-d_8 exhibits three well-separated resonances of an AA′XX′Y spin system, consistent with a coordination environment of five phosphorus donors. The measured and simulated $^{31}P\{^1H\}$ NMR spectra are shown in Figure 2. A multiplet resonance at δ 64.5 corresponds to the phosphorus atoms of the dmpe ligand, while the two phosphorus atoms of the $P^{Ph}{}_3N^{Bn}{}_3$ ligand positioned trans to dmpe are located at δ 44.1. The resonance at δ 38.1 corresponds to the third phosphorus atom of the $P^{Ph}{}_3N^{Bn}{}_3$ ligand that is trans disposed to the N_2 ligand.

The $^{15}N_2$-labeled isotopologue **2(^{15}N$_2$)** was initially prepared in a similar way to eq 1, under an atmosphere of $^{15}N_2$ gas. After the reaction workup under an ambient N_2 atmosphere, it became apparent that Cr−$^{15}N_2$ ligand exchange with $^{14}N_2$ is facile, resulting in the loss of the labeled $^{15}N_2$ ligand. Therefore, the workup of subsequent reactions to prepare **2(^{15}N$_2$)** in a similar way to eq 1 was performed under an atmosphere of argon. Alternatively, **2(^{15}N$_2$)** can be conveniently generated by rigorously mixing a degassed sample of **2(N$_2$)** in THF under an atmosphere of $^{15}N_2$ gas. The $^{15}N\{^1H\}$ NMR spectrum of **2(^{15}N$_2$)** (referenced to $CH_3{}^{15}NO_2$) recorded in THF-d_8 contains a broad resonance (due to ^{31}P coupling) at δ −10.3 and a doublet at δ −14.5 (J_{NN} = 7 Hz) for the proximal and distal nitrogen atoms of the end-on $^{15}N_2$ ligand, respectively, Figure 3.

The ^{15}N NMR chemical shift values for **2(^{15}N$_2$)** are not particularly informative for evaluating the extent of activation of the N_2 ligand. However, combining the current data with results of our earlier spectroscopic studies of Cr−N_2 complexes, a more complete periodic trend of ^{15}N chemical shifts for the N_2 ligands of group 6 dinitrogen complexes bearing end-on N_2 ligands can be established. Table 1 contains ^{15}N NMR data for **2(^{15}N$_2$)**, two Cr^0 bis(dinitrogen) complexes prepared in our laboratory (*cis*-[Cr($^{15}N_2$)$_2$($P^{Ph}{}_2N^{Bn}{}_2$)$_2$],[15] *trans*-[Cr($^{15}N_2$)$_2$($P^{Ph}{}_4N^{Bn}{}_4$)],[16]), and new ^{15}N NMR data for *trans*-[Cr($^{15}N_2$)$_2$(dmpe)$_2$],[17] (^{15}N NMR data not previously reported, see Supporting Information). All of the $^{15}N_2$-labeled bis(dinitrogen) Cr complexes exhibit ^{15}N chemical shifts that are located downfield (less shielded) compared to bis(dinitrogen) Mo and W−$^{15}N_2$ compounds. This trend is consistent with a study by Mason and Richards that examined periodic trends in the ^{15}N NMR chemical shifts of transition metal dinitrogen complexes bearing end-on $^{15}N_2$ ligands.[27] For example, in the analysis of complexes containing identical diphosphine ligands, such as *trans*-[M($^{15}N_2$)$_2$(P-P)$_2$] (M = Mo, W; P-P = $Et_2PCH_2CH_2PEt_2$ (depe), $Ph_2PCH_2CH_2PPh_2$ (dppe)), the ^{15}N chemical shifts of both ^{15}N atoms of $^{15}N_2$ moved upfield with an increase in the atomic number of the metal. This observation was attributed to an increase in ligand nuclear magnetic shielding going down the group.[27] Unfortunately, a comparison of the respective Cr analogues to the Mo and W bis(dinitrogen) complexes listed above bearing chelating diphosphine ligands cannot be made, as Cr bis(dinitrogen) analogues of depe or dppe[38] have not been prepared. To the best of our knowledge, *cis*-[M(N_2)$_2$(PMe_3)$_4$], (M = Cr, Mo, W) is the only known series of group 6 dinitrogen compounds with a common supporting phosphorus ligand environment.[24,31,37] While ^{15}N NMR data has not been reported for this series of complexes, Carmona and co-workers noted a linear correlation of the ^{31}P resonances (moving upfield) with increasing atomic number.[37] In the current study ^{15}N NMR resonances for the proximal and distal nitrogen atoms of the $^{15}N_2$ ligand in **2(^{15}N$_2$)** also appear downfield compared to structurally similar Mo mono-dinitrogen complexes with a pentaphosphine coordination environment comprised of a tridentate and bidentate ligand (summarized in Table 1). Thus, although there is currently a limited amount of ^{15}N NMR data available, a similar periodic trend is apparent for complexes with a phosphorus donor located trans to the N_2 ligand.

The cyclic voltammogram (CV) of **2(N$_2$)** was recorded in THF at a scan rate of 0.10 V/s and exhibits two, one-electron redox events, Figure 4. The $E_{1/2}$ for the reversible $Cr^{I/0}$ redox couple appears at −1.50 V, reflecting a particularly electron-rich metal center. For comparison, the cyclic voltammograms recorded at a scan rate of 0.10 V/s of the previously reported Cr bis(dinitrogen) complexes *trans*-[Cr(N_2)$_2$($P^{Ph}{}_4N^{Bn}{}_4$)][16] and *cis*-[Cr(N_2)$_2$($P^{Ph}{}_2N^{Bn}{}_2$)$_2$] exhibit an irreversible $Cr^{I/0}$ wave at E_{pa} = −1.10 V. It is evident that the pentaphosphorus coordination environment stabilizes the oxidized $[Cr^I\text{-}N_2]^+$ species compared to the Cr bis(dinitrogen) counterparts. Upon scanning to a more positive potential, an irreversible oxidation wave at E_{pa} = −0.77 V is assigned as the $Cr^{II/I}$ couple. The irreversible nature of this wave is likely a result of N_2 ligand loss from an unstable $[Cr^{II}\text{-}N_2]^{2+}$ species. The small feature at ∼ −1.3 V observed in the cathodic scan is likely related to N_2 loss from $[Cr^{II}\text{-}N_2]^{2+}$, as it is present only after scanning to the positive potential of the $Cr^{II/I}$ feature. It is plausible that this feature corresponds to the reduction of a Cr^{II}-THF species that is formed upon N_2 dissociation (see Supporting Information for additional CV data). Notably, the CV data of **2(N$_2$)** closely resemble the appearance of voltammograms for bis(dinitrogen)

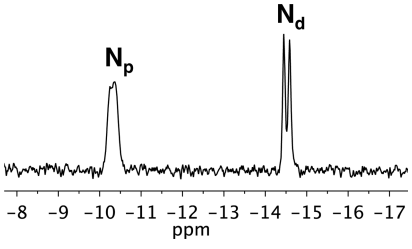

Figure 3. $^{15}N\{^1H\}$ NMR spectrum of **2(^{15}N$_2$)** recorded at 21 °C in THF-d_8. Resonances at δ −10.3 and δ −14.5 (J_{NN} = 7 Hz) correspond to the proximal (N_p) and distal (N_d) nitrogen atoms, respectively, of the end-on $^{15}N_2$ ligand.

DOI: 10.1021/acs.inorgchem.5b00351
Inorg. Chem. 2015, 54, 4827−4839

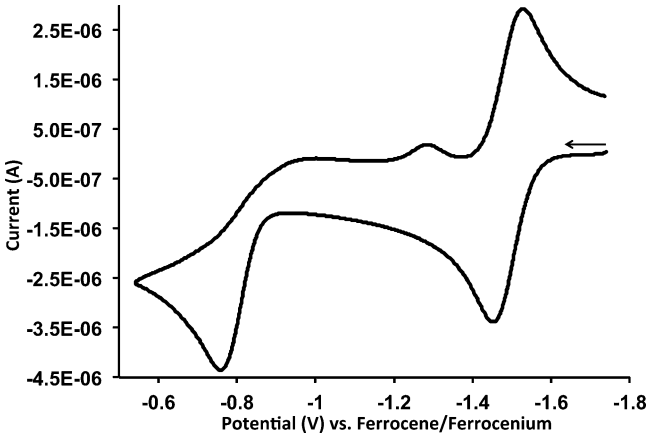

Figure 4. Cyclic voltammogram recorded at 22 °C showing the reversible $Cr^{I/0}$ and irreversible $Cr^{II/I}$ couple of $Cr(N_2)(dmpe)(P^{Ph}{}_3N^{Bn}{}_3)$ (**2(N$_2$)**) in THF. Scan rate = 0.10 V/s, supporting electrolyte of 0.2 M $[NBu_4][B(C_6F_5)_4]$.

complexes of the type $M(N_2)_2(PNP)_2$, (M = Mo, W; PNP = $[(R_2PCH_2)_2N(R')$, R = Et, Ph; R′ = Me, Bn]), which exhibit a reversible $M^{I/0}$ couple and irreversible $M^{II/I}$ couple on the CV time-scale at 0.10 V/s.[35,39] No reduction waves were observed for **2(N$_2$)** in a cathodic scan from −1.7 V to the end of the solvent window (∼ −3.0 V).

The increased activation of the coordinating N_2 ligand due to the electron-rich Cr center is in accord with our previous computational electronic structure analysis that described the nature of the Cr−N_2 bonding interaction. Our results, based on calculations of the *cis*-$[Cr(N_2)_2(P^{Ph}{}_2N^{Bn}{}_2)_2]$, revealed that a buildup of electron density around Cr leads to an increased polarization of the N_2 ligand, resulting in both N−N bond elongation and a decrease of the N_2 vibrational frequency.[15] We postulate from the observed oxidation potential for **2(N$_2$)** that the combination of electron-donating phosphine ligands (i.e., dmpe) and the phosphorus donor trans to the N_2 ligand enhances the activation of the N_2 ligand, and we evoked a similar rationalization for a polarization of N_2 as in our quantitative description of the bonding in Cr−N_2 and $FeX(N_2)(P^{Et}N^{Me}P^{Et})_2$ (X = Cl, H) systems.[40]

Protonation Studies of 2(N$_2$). Encouraged by the spectroscopic data suggesting a strongly activated N_2 ligand in **2(N$_2$)**, we performed a qualitative assessment of the reactivity with acid to investigate the preferred protonation sites and test for the stoichiometric generation of hydrazine and/or ammonia. NMR spectroscopic studies employed the $^{15}N_2$-labeled complex **2(^{15}N$_2$)**. Treatment of **2(^{15}N$_2$)** with 1 equiv of $[H(OEt_2)_2][B(C_6F_5)_4]$ in THF-d_8 at −78 °C resulted in the immediate protonation of the Cr^0 center producing, to the best of our knowledge, the first example of a seven-coordinate Cr^{II} dinitrogen hydride complex, $[Cr(H)(^{15}N_2)(dmpe)(P^{Ph}{}_3N^{Bn}{}_3)][B(C_6F_5)_4]$ ($[$**2(H)(^{15}N$_2$)**$]^+$), (eq 2).([**2-**

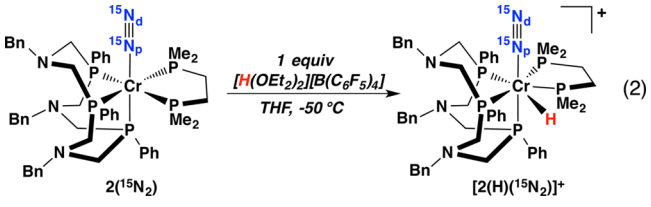

(2)

$[$**2(H)(^{15}N$_2$)**$]^+$) can also be prepared by the stoichiometric addition of triflic acid, although the concomitant formation of a minor amount of an unidentified product was observed by ^{31}P NMR spectroscopy. The ^{1}H NMR spectrum recorded at −50 °C features an apparent sextet at δ −6.3 for the hydride resonance. Resonances at δ −9.6 and −28.9 in the ^{15}N NMR spectrum (Figure 5) are assigned to the distal (N_d) and

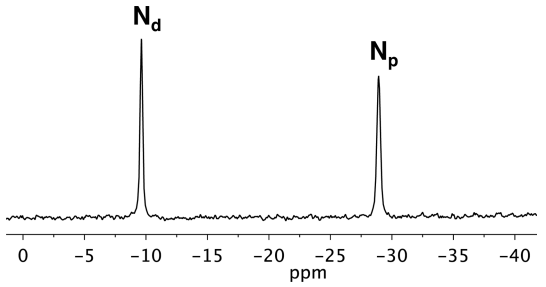

Figure 5. $^{15}N\{^1H\}$ NMR spectrum of $[$**2(H)(^{15}N$_2$)**$]^+$ recorded at −50 °C in THF-d_8. Resonances at δ −9.6 and δ −28.9 correspond to the distal (N_d) and proximal (N_p) nitrogen atoms, respectively, of the end-on $^{15}N_2$ ligand.

proximal (N_p) nitrogen atoms of $^{15}N_2$, respectively. Although the J_{NN} coupling was not observed for the distal nitrogen atom as it was identified in the ^{15}N NMR spectrum of the parent dinitrogen complex **2(^{15}N$_2$)**, the broadness of the signal at δ −28.9 suggests coupling to the ^{31}P nuclei, aiding assignment of this resonance as N_p. Notably, the chemical shifts of the N_d and N_p atoms are reversed in $[$**2(H)(^{15}N$_2$)**$]^+$ compared to the parent dinitrogen complex **2(^{15}N$_2$)**, possibly a consequence of a less electron-rich Cr center upon hydride formation.

Variable temperature $^{31}P\{^1H\}$ NMR data, shown in Figure 6, suggest a nonrigid, seven-coordinate structure in solution[41] based on broad ^{31}P signals between −30 and −60 °C. $[$**2(H)(^{15}N$_2$)**$]^+$ could adopt structures that include a pentagonal bipyramid or a capped octahedral geometry[42] as observed in seven-coordinate Cr, Mo, and W dicarbonyl systems.[43] At −30 °C the ^{31}P spectrum contains three features, two broad resonances at δ 62.0 and 26.8, assigned to dmpe and $P^{Ph}{}_3N^{Bn}{}_3$ ligands, respectively, and a sharp pentet at δ 35.9, corresponding to the axial phosphorus atom of the $P^{Ph}{}_3N^{Bn}{}_3$ ligand.

Cooling the sample below −30 °C resulted in further broadening of the already broad singlet resonances, while the appearance of the pentet was not significantly broadened until −72 °C. At −60 °C, the resonances at δ 62.0 and 26.8 are nearly completely broadened into the baseline. Further cooling to −72 °C resulted in the appearance of four broad features (see Supporting Information for a ^{31}P NMR spectrum with an increased vertical scale), indicating decoalescence of the ^{31}P resonances at this temperature due to slowed fluxional behavior. At temperatures greater than −30 °C, $[$**2(H)(^{15}N$_2$)**$]^+$ is unstable for extended periods of time. For example, maintaining the temperature of the sample at −30 °C for 9 h resulted in loss of ^{31}P resonances of $[$**2(H)(^{15}N$_2$)**$]^+$ and the appearance of broad signals in the ^{1}H NMR spectrum, presumably due to a paramagnetic complex, as well as a resonance for free $^{15}N_2$ in the ^{15}N NMR spectrum. Since no resonances for free phosphine ligands were observed, it is presumed that loss of the N_2 ligand was accompanied by a spin-state change and the formation of an unidentified paramagnetic, but likely hydride-containing product.

DOI: 10.1021/acs.inorgchem.5b00351
Inorg. Chem. 2015, 54, 4827−4839

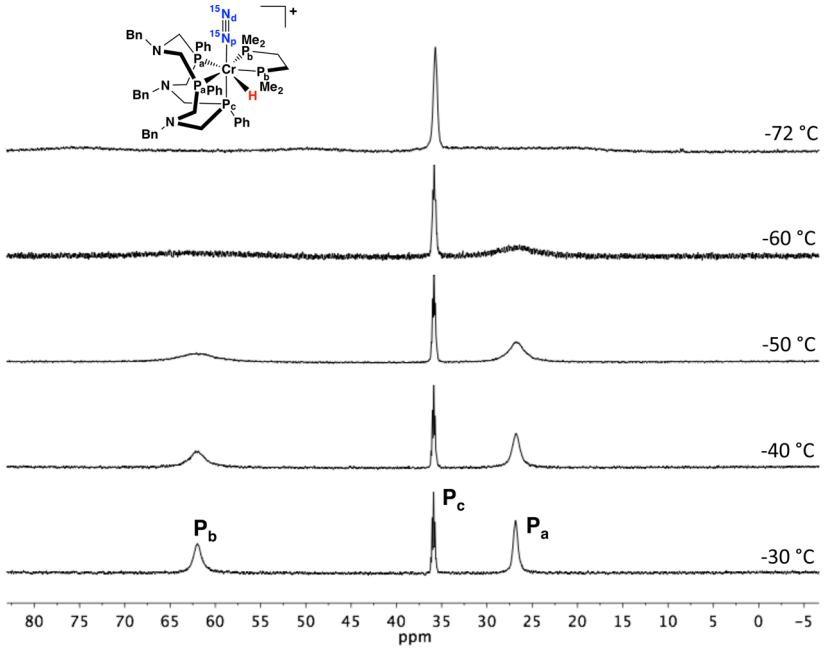

Figure 6. Variable temperature $^{31}P\{^{1}H\}$ NMR spectra of $[\mathbf{2(H)(^{15}N_2)}]^+$ recorded in THF-d_8 from −30 to −72 °C.

Protonation of $\mathbf{2(N_2)}$ was also monitored by *in situ* IR spectroscopy, Figure 7. Treatment of $\mathbf{2(N_2)}$ with 1 equiv of

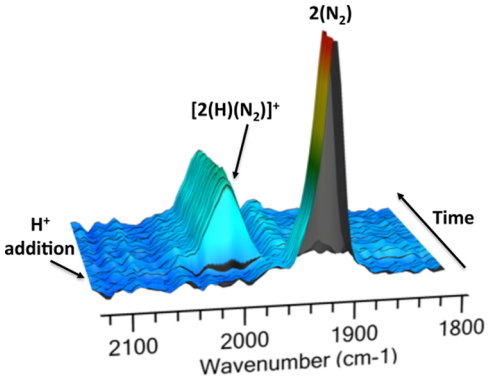

Figure 7. *In situ* IR plot recorded in THF at −78 °C showing the formation of $[\mathbf{2(H)(N_2)}]^+$ from the reaction of $\mathbf{2(N_2)}$ with 1 equiv $[H(OEt_2)_2][B(C_6F_5)_4]$. Data collected in 15 s increments.

$[H(OEt_2)_2][B(C_6F_5)_4]$ at −78 °C shows an immediate increase of 88 cm^{-1} in the frequency of the ν_{NN} band from 1918 to 2006 cm^{-1}, corresponding to the formation of $[\mathbf{2(H)(N_2)}]^+$. The protonation of the Cr center and subsequent increase in the oxidization state of Cr by two electrons results in a less electron-rich metal center and a substantially less activated N_2 ligand.

The formation of seven-coordinate Mo and W bis(dinitrogen) complexes has been previously encountered by our group in systems supported by phosphine ligands that contain pendant amines.[44,45] For example, the addition of HOTf to *trans*-$[W(N_2)_2(dppe)(P^{Et}N^{Me}P^{Et})]$ (dppe = $Ph_2PCH_2CH_2PPh_2$; $P^{Et}N^{Me}P^{Et}$ = $Et_2PCH_2N(Me)CH_2PEt_2$) afforded *trans*-$[W(N_2)_2(H)(dppe)(P^{Et}N^{Me}P^{Et})][OTf]$.[44] In this study, we noted that acid treatment of the complex lacking a pendant amine group, *trans*-$[W(N_2)_2(dppe)(depp)]$ (depp = $Et_2P(CH_2)_3PEt_2$), selectively formed the hydrazido complex *trans*-$[W(NNH_2)(OTf)(dppe)(depp)][OTf]$. The difference in the final protonated products was attributed to the pendant amine group being the kinetic site of protonation (due to their location in the second coordination sphere) and capable of providing a pathway for intramolecular proton movement to the thermodynamically preferred protonation site, the metal center. In the present case, although we did not prepare a derivative of a pentaphosphine mono-dinitrogen complex of Cr that lacks the pendant amine groups to compare acid reactivity, we postulate that $[\mathbf{2(H)(N_2)}]^+$ is formed by a similar intramolecular proton transfer pathway, where a proton could rapidly transfer from one of three pendant amine groups in the second coordination sphere to the electron-rich Cr center (see Computational Analysis section below for more details).

To examine whether protonation of $\mathbf{2(^{15}N_2)}$ would result in the formation of hydrazinium or ammonium, $\mathbf{2(^{15}N_2)}$ was treated with 12 equiv of HOTf in THF at −78 °C, eq 3.

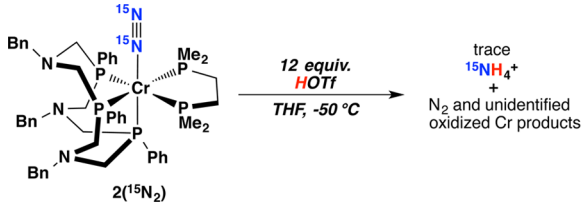

(3)

Hydrazinium or ammonium was not detected by ^{15}N NMR spectroscopy after 2 h. After 24 h at −50 °C the $^{15}N\{^{1}H\}$ NMR spectrum showed no signals corresponding to a metal-bound $^{15}N_2$ ligand, indicating disappearance of $\mathbf{2(^{15}N_2)}$. After this time, the only detectible product in the $^{15}N\{^{1}H\}$ NMR spectrum was free $^{15}N_2$ (δ −71) and a resonance for $^{15}NH_4^+$ at δ −364, indicating a trace amount of $^{15}NH_4^+$ was formed from reduction of the $^{15}N_2$ ligand (see Supporting Information for $^{15}N\{^{1}H\}$ and $^{1}H-^{15}N$ HSQC NMR spectra). To quantify the NH_4^+ generated in this reaction the indophenol method was employed (see Experimental Section for details). A stirring solution of $\mathbf{2(N_2)}$ in a Schlenk flask was treated with 20 equiv of HOTf in THF at −78 °C and maintained at this temperature

DOI: 10.1021/acs.inorgchem.5b00351
Inorg. Chem. 2015, 54, 4827−4839

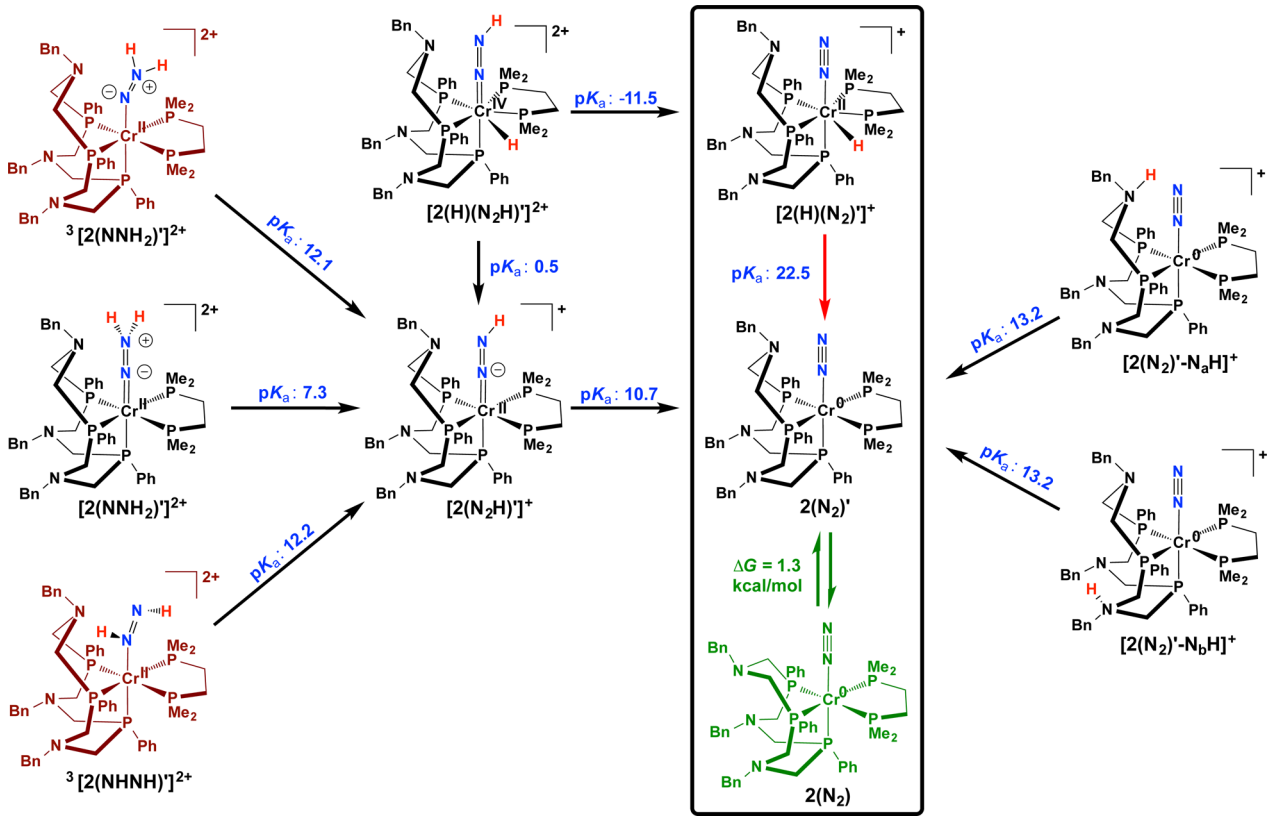

Figure 8. Computed pK_a values and protonation pathways for various sites of **2(N$_2$)**. The red structures on the top and bottom left signify a triplet spin-state of Cr. The boxed species are those involved in the predominant pathway (green arrows indicate the *exo*/*endo* isomerization of the pendant amine and the red arrow indicates the thermodynamically preferred Cr−H formation).

for 21 h, and then stirred at −40 °C for 2 h before warming to room temperature. Consistent with the NMR experiments, only a trace amount (<1%) of ammonia was detected (not quantifiable by the indophenol method). Hydrazine was not detected as a product in this reaction. Initial experiments were conducted to test for catalytic ammonia production using **2(N$_2$)** as a precatalyst by the metered addition of lutidinium triflate in toluene over 3 h, to a hexanes solution containing **2(N$_2$)** and decamethylchromocene ($Cr(C_5Me_5)_2$) at −78 °C, followed by stirring for 36 h.[11,12] However, in these experiments only trace amounts of ammonium were formed, as determined by the indophenol method.

Computational Analysis. To understand the origin of the reactivity with respect to ammonium formation of **2(N$_2$)** and compare it to the recently reported *trans*-$[Cr(N_2)_2(P^{Ph}{}_4N^{Bn}{}_4)]$ complex, we have undertaken detailed electronic structure based studies of the protonation and reduction of N_2 on both complexes. We note that the latter complex also produced ammonium in trace amounts when exposed to excess triflic acid, but with the distinct difference that hydrazinium is also observed as the predominant product. In accord with the experimental observations, the simulations also find **2(N$_2$)** to exist in the singlet state, and all computations retain this multiplicity unless otherwise stated.

The optimized geometry of **2(N$_2$)′** (prime denotes computationally derived structures) is in good agreement with the X-ray crystal structure (see Supporting Information). Computationally, two distinct conformers were denoted, depending on the conformation of the macrocycle with respect to the position of the pendant amine: *endo* isomers are defined to have the pendant amine lone pair oriented toward the bound N_2 (and Cr), whereas *exo* isomers (as seen in the X-ray structure) orient the amine lone pair away from the bound N_2. Although the *exo* conformer of the pendant amine closest to the bound N_2 is observed in the solid-state, the *endo* conformer was considered for pK_a calculations for two reasons: (1) upon protonation, the *endo* isomer would more easily define a pathway for proton transfer to N_2 (i.e., **[2(N$_2$)′-N$_a$H]$^+$** to **[2(N$_2$H)′]$^+$**; Figure 8) and (2) conversion between *exo* and *endo* isomers should occur readily as the isomerization barrier (1.1 kcal/mol), and the small free energy difference (1.3 kcal/mol) suggest the two species will be in equilibrium in solution. There are four protonation sites considered in the calculations of **2(N$_2$)′**: the Cr center (**[(2(H)(N$_2$)′]$^+$**), the distal nitrogen of N_2 (**[2(N$_2$H)′]$^+$**, the pendant amine closest to N_2, (**[2(N$_2$)′-N$_a$H]$^+$**), and the remaining pendant amine sites (**[2(N$_2$)′-N$_b$H]$^+$** (for simplicity the other symmetrically equivalent amine was not considered). The Cr center is the most basic site (red arrow in Figure 8; **[(2(H)(N$_2$)′]$^+$** pK_a = 22.5) in accord with the experimental observation that 1 equiv of acid leads to a seven-coordinate hydride species (eq 2). The next most basic site is the pendant amines (**[2(N$_2$)′-N$_a$H]$^+$**/**[2(N$_2$)′-N$_b$H]$^+$**; pK_a = 13.2), while the least basic site is the N_2 ligand (**[2(N$_2$H)′]$^+$**; pK_a = 10.7). While the metal center is thermodynamically preferred, we note that the location of the pendant amines in the second coordination sphere are likely the kinetic sites of protonation and could provide an avenue for intramolecular proton transfer to the metal center. Protonation at Cr results in a dramatic decrease the basicity of the distal nitrogen atom of the N_2 ligand. For example, DFT analysis predicts the pK_a of the N_2 site in **[2(H)(N$_2$H′)]$^{2+}$** to be −11.5,

DOI: 10.1021/acs.inorgchem.5b00351
Inorg. Chem. 2015, 54, 4827−4839

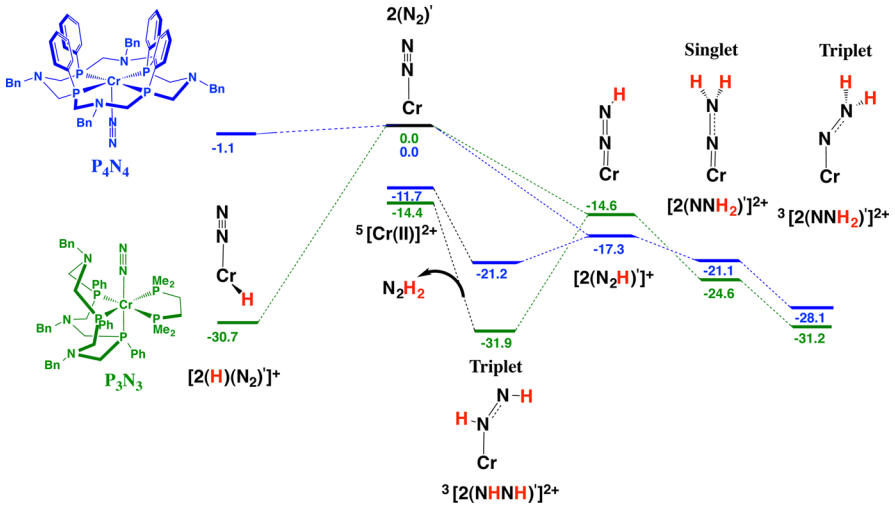

Figure 9. Free energy diagram (kcal/mol) for Cr and N_2 protonation for $\mathbf{2(N_2)'}$ (green) and $\mathbf{3(N_2)'}$ (blue).

which suggests additional protonation events at the N_2 ligand following metal protonation are highly unfavorable.

The basicities of the Cr and N_2 sites may be directly compared to the corresponding sites in our previously reported Cr dinitrogen complex *trans*-$[Cr(N_2)_2(P^{Ph}{}_4N^{Bn}{}_4)]$.[18] To enable a direct comparison with $\mathbf{2(N_2)'}$, containing one N_2 ligand, the five-coordinate species $Cr(N_2)(P^{Ph}{}_4N^{Bn}{}_4)$ ($\mathbf{3(N_2)'}$) is considered in the calculations. Although dissociation of one N_2 ligand from *trans*-$[Cr(N_2)_2(P^{Ph}{}_4N^{Bn}{}_4)]$ requires 12.1 kcal/mol in energy, $\mathbf{3(N_2)'}$ was proposed by earlier DFT studies to activate N_2 sufficiently to produce hydrazine and trace amounts of ammonia upon addition of HOTf.[16] The high basicity of Cr in $\mathbf{2(N_2)'}$ is in marked contrast to that of $[\mathbf{3(H)(N_2)'}]^+$ (pK_a = 0.8). This difference is attributed predominantly to the presence of the more electron-rich phosphorus coordination sphere, particularly the dmpe ligand and the phosphorus donor that is trans to the bound N_2 in $\mathbf{2(N_2)}$, which, as noted above, increases the electron density at the Cr center and in turn enhances the stability of the hydride species, $[\mathbf{(2(H)(N_2)'}]^+$.

Regardless of the undesired Cr protonation observed in $\mathbf{2(N_2)'}$, there are marked differences in the thermodynamically preferred products formed upon protonation N_2 in these two systems.[16] In the initial protonation to form the diazenido intermediate $[\mathbf{2(N_2H)'}]^+$, the acidity of the protonated distal N atom is predicted to be similar ($[\mathbf{2(N_2H)'}]^+$: pK_a = 10.7; $[\mathbf{3(N_2H)'}]^+$: pK_a = 12.7).[46] However, when a second protonation step occurs to form the hydrazido species ($[\mathbf{2(NNH_2)'}]^{2+}$; Figure 8), the distal N atom is more acidic than $[\mathbf{3(NNH_2)'}]^{2+}$ (pK_a = 2.8) but significantly less acidic in $[\mathbf{2(NNH_2)'}]^{2+}$ (pK_a = 7.3). Initial protonation for both complexes results in the shortening of the Cr−N bond from 1.9 ($[\mathbf{2(N_2H)'}]^+$) or 1.8 ($[\mathbf{3(N_2H)'}]^+$) Å to 1.7 Å and an increase of the N−N bond from 1.1 to 1.2 Å, consistent with a Cr═N═N−H resonance structure which would result in a formal oxidation state of Cr^{II}.[16] In this context, the lower acidity of the hydrazido unit in $[\mathbf{2(NNH_2)'}]^{2+}$ can be viewed as a consequence of enhanced stabilization of the Cr^{II} center by the phosphine *trans* to the hydrazido ligand. Upon protonation of the diazenido to give the hydrazido species, the calculated Cr═N bond length decreases by ∼0.1 Å and the N═N distance increases by ∼0.1 Å. Furthermore, in either system the distal nitrogen of the hydrazido ligand is even less acidic provided that accompanying the second protonation, a spin transition to a more stable triplet hydrazido intermediate occurs (pK_a = 12.1 and 6.5 for $(^3[\mathbf{2(NNH_2)'}]^{2+}$ and $(^3[\mathbf{3(NNH_2)'}]^{2+}$, respectively) ($\Delta G_{(singlet\rightarrow triplet)}$: −6.6 ($P_3N_3$) and −7.0 ($P_4N_4$) kcal/mol), shown in Figure 9.

Compared with the singlet hydrazido geometry, the N−N distance for the triplet species differs by <0.02 Å, while the Cr−N the bond length is larger by 0.1 Å (1.7−1.8 and 1.6−1.7 Å in P_3N_3 and P_4N_4, respectively), suggesting a Cr−N═NH_2 resonance structure. Furthermore, the Cr−N−N unit is no longer linear as in the singlet (177.5° ($[\mathbf{2(NNH_2)'}]^{2+}$) and 175.3° ($[\mathbf{3(NNH_2)'}]^{2+}$)), but bent (143.9° ($^3[\mathbf{2(NNH_2)'}]^{2+}$) and 143.8° ($^3[\mathbf{3(NNH_2)'}]^{2+}$)), Figure 9. Spin crossover, then, is a likely occurrence in these complexes at higher levels of protonation and is driven thermodynamically by the enhanced stability of the doubly protonated intermediates. In addition to hydrazido intermediates, spin crossover for a second protonation of $[\mathbf{2(N_2H)'}]^+$ at the proximal nitrogen to form a triplet symmetric diazene intermediate[47] ($^3[\mathbf{2(NHNH)'}]^{2+}$) is also energetically favorable; however, because protonation at the distal nitrogen, i.e., ($[\mathbf{2(N_2H)'}]^+ \rightarrow [\mathbf{2(NNH_2)'}]^{2+}$), can proceed on the singlet surface (i.e., a spin allowed transition) the former pathway is less favorable. Nevertheless, if the triplet diazene intermediate ($^3[\mathbf{2(NHNH)'}]^{2+}$) is formed, the Cr−N bond is elongated by 0.07 Å (P_3N_3) and 0.05 Å (P_4N_4) relative to the Cr−N bond in $\mathbf{2(N_2)'}$. The dissociation of N_2H_2 can lead to hydrazine formation upon disproportionation ($2\ N_2H_2 \rightarrow N_2H_4 + N_2$)[48] by well-established chemistry. Such a process is more favored for the P_4N_4 system than the P_3N_3 system (ΔG = 9.5 (P_4N_4) vs 17.5 (P_3N_3) kcal/mol), which is consistent with the finding that treatment of *trans*-$[Cr(N_2)_2(P^{Ph}{}_4N^{Bn}{}_4)]$ with excess HOTf preferentially forms $N_2H_5^+$,[16] whereas with $\mathbf{2(N_2)}$, only trace NH_4^+ is observed under similar conditions. To interrogate this variance in protonated products in the two systems, we examined the possibility of a spin-state crossover in the doubly protonated hydrazido complexes $[\mathbf{2(NNH_2)'}]^{2+}$ and $[\mathbf{3(NNH_2)'}]^{2+}$. However, we conclude that a singlet to triplet crossover alone does not explain the difference in reactivity between the P_3N_3 and P_4N_4 based complexes. Computational details on the singlet to triplet transition for $[\mathbf{2(NNH_2)'}]^{2+}$ and $[\mathbf{3(NNH_2)'}]^{2+}$ are provided in the Supporting Information.

In order to gain a more detailed understanding of the slow rates and reaction selectivity of $NH_4^+/N_2H_5^+$ production, we explored the mechanistic pathways of N_2 reduction from the

DOI: 10.1021/acs.inorgchem.5b00351
Inorg. Chem. 2015, 54, 4827−4839

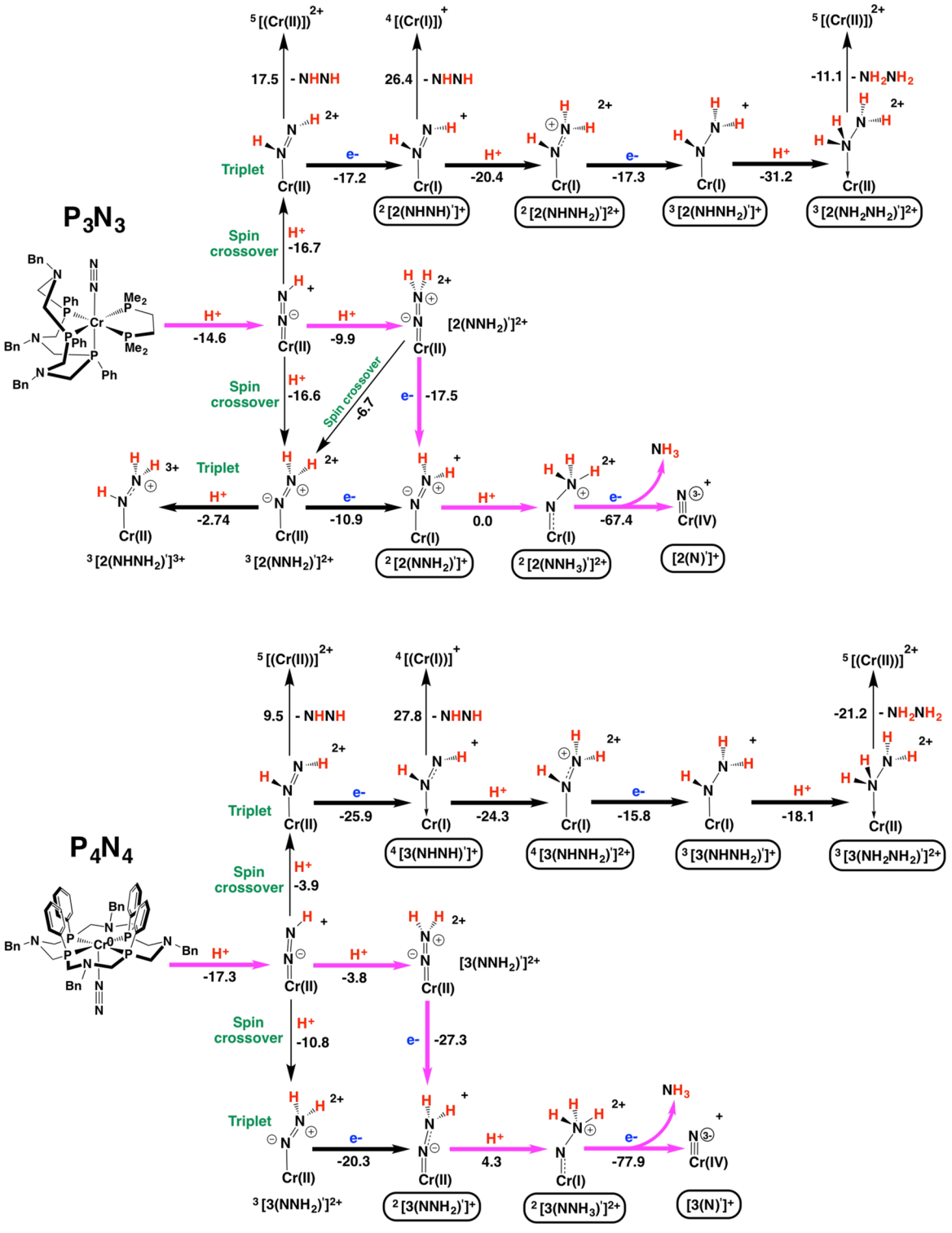

Figure 10. Free energies (kcal/mol) for N_2 protonation and reduction steps in $\mathbf{2}(\mathbf{N_2})'$ (top) and $\mathbf{3}(\mathbf{N_2})'$ (bottom). The thermodynamically preferred pathway on the singlet surface is shown in pink. Thick and thin arrows correspond to energetically favorable spin allowed and spin forbidden steps, respectively.

addition of electrons to the Cr-N_xH_y intermediates described above for both systems. We note that this is a distinct possibility in these systems since a neutral (not protonated) or cationic (monoprotonated) species present in solution may serve as a reducing agent for species with higher positive charge. Upon formation of the diazene or hydrazido intermediates the addition of a third proton is unfavorable, as the calculated hydrazinium species (Cr-N-NH_3) exhibits negative pK_a values. In our previous computational evaluation of $\mathbf{3}(\mathbf{N_2})'$,[16] we postulated that forming $^3[\mathbf{3}(\mathbf{NHNH})']^{2+}$ could lead to the dissociation of diazene (N_2H_2) from Cr, which could disproportionate to form hydrazine and N_2. By contrast, this process is less likely in $^3[\mathbf{2}(\mathbf{NHNH})']^{2+}$, where diazene binding is computed to be stronger by 8.0 kcal/mol, Figure 10.

DOI: 10.1021/acs.inorgchem.5b00351
Inorg. Chem. 2015, 54, 4827−4839

However, if a reduction step occurs it is possible to further protonate the hydrazido and diazene species and liberate NH_3 or N_2H_4 for P_3N_3 and P_4N_4, respectively. The comparative energetics for N_2 protonation/reduction leading to ammonia release is given in Figure 10 for both P_3N_3 and P_4N_4 systems.

For this analysis, free energies for electron addition steps are computed with respect to the $(Cp^*)_2Cr \rightarrow (Cp^*)_2Cr^+ + e^-$ half-reaction ($Cp^* = \eta^5$-C_5Me_5). For each of the intermediates shown in Figure 10, the optimized geometries of the central Cr-N-N (and the assigned resonance structures and formal oxidation states), with the exception of $^2[\mathbf{2}(\mathbf{NNH_2})']^+$, are similar in both P_3N_3 and P_4N_4 systems. The geometry of the Cr-N-N unit in the hydrazido intermediate $^2[\mathbf{2}(\mathbf{NNH_2})']^+$ (bent Cr-N═N (P_3N_3) and linear Cr═N-N (P_4N_4)), on the other hand, is dependent on the P4 vs P5 coordination sphere about Cr.[49] The energetically preferred pathway also shows little dependence on supporting ligand (pink arrows) and entails (1) double protonation of N_2 to yield a hydrazido intermediate $[\mathbf{2}(\mathbf{NNH_2})']^{2+}$ followed by (2) one-electron reduction to a monocationic hydrazido intermediate $^2[\mathbf{2}(\mathbf{NNH_2})']^+$ (ΔG = −17.5 (P_3N_3) and −27.3 (P_4N_4) kcal/mol) after which (3) a third protonation becomes feasible (ΔG = 0.0 (P_3N_3) and 4.3 (P_4N_4) kcal/mol), affording a hydrazidium species $^2[\mathbf{2}(\mathbf{NNH_3})']^{2+}$ from which NH_3 formation occurs upon reduction ($\Delta G < -67$ kcal/mol), affording a Cr-nitrido product $[\mathbf{2}(\mathbf{N})']^+$. Reduction of the doubly protonated hydrazido intermediate is more facile for P_4N_4 than for P_3N_3 by 9.8 kcal/mol due to the less electron-rich metal center of the former, but subsequent protonation remains thermodynamically uphill by 4.3 kcal/mol. Both species, however, will spontaneously release NH_3 upon a third protonation followed by addition of an electron. Thus, according to our computational results, the fundamental difference between the two systems is that reduction of the Cr center should be the thermodynamic bottleneck in the P_3N_3 system (which could be overcome by using a stronger chemical reductant), whereas protonation should be the main bottleneck for the P_4N_4 system.

The overall picture that emerges from our computational analysis of the energetics of the various isomers of mono- and diprotonation is that unlike $\mathbf{3}(\mathbf{N_2})'$, $\mathbf{2}(\mathbf{N_2})'$ can result in favorable mono- and diprotonation of bound N_2 as the more electron-rich Cr center helps to stabilize these intermediates. However, this electron-rich Cr leads to a strong thermodynamic preference to form the seven-coordinate $Cr(N_2)$ hydride species $[(\mathbf{2}(\mathbf{H})(\mathbf{N_2})']^+$, resulting in a competing pathway with N_2 protonation. This observation qualitatively rationalizes the overall slow rate and low yield of NH_3 upon addition of excess acid to $\mathbf{2}(\mathbf{N_2})$. On the other hand, $\mathbf{3}(\mathbf{N_2})'$ is hindered by a less basic N_2 moiety and a slow singlet to triplet crossover rate. Ultimately for this latter complex, even though there is a route to directly release NH_3 via reduction, this pathway will be in competition with dissociation of N_2H_2 from $^3[\mathbf{3}(\mathbf{NHNH})']^{2+}$; an avenue which (as noted in the Supporting Information) is less favored in the P_3N_3 system.

CONCLUSIONS

We report the synthesis, characterization, and acid reactivity of the mono-dinitrogen Cr^0 complex, $Cr(N_2)(dmpe)(P^{Ph}{}_3N^{Bn}{}_3)$, $\mathbf{2}(\mathbf{N_2})$, containing a pentaphosphine coordination environment; the first example of a pentaphosphine Cr-N_2 complex. Infrared and X-ray diffraction data suggest a modestly activated terminal N_2 ligand as a result of an electron-rich Cr center. Treatment of $\mathbf{2}(\mathbf{N_2})$ at −78 °C with 1 equiv of $[H(OEt_2)_2][B(C_6F_5)_4]$ affords a seven-coordinate Cr^{II}-N_2 hydride complex, $[Cr(H)(N_2)(dmpe)(P^{Ph}{}_3N^{Bn}{}_3)][B(C_6F_5)_4]$, $[\mathbf{2}(\mathbf{H})(\mathbf{N_2})]^+$. Further, treatment of $\mathbf{2}(^{15}\mathbf{N_2})$ with excess triflic acid at −50 °C afforded only a trace amount of $^{15}NH_4^+$ from the reduction of the coordinated $^{15}N_2$ ligand. Computational studies were employed to examine the thermodynamically preferred protonation sites of $\mathbf{2}(\mathbf{N_2})$. These results indicate a strong thermodynamic preference to protonate the metal center, consistent with experimental results, which is a competing pathway to N_2 protonation in this system. In addition, the N_2 reduction pathways resulting from the addition of protons and electrons to Cr-N_2 complexes bearing the $P^{Ph}{}_3N^{Bn}{}_3$ and $P^{Ph}{}_4N^{Bn}{}_4$ ligands were examined computationally to rationalize differences in their reactivity profiles. These studies predict the more electron-rich metal center in the pentaphosphine coordination sphere for $\mathbf{2}(\mathbf{N_2})$ leads to a thermodynamically more favorable route to form NH_3 via an asymmetric N_2 reduction pathway (sequential protonation of the distal N atom) compared to $\mathbf{3}(\mathbf{N_2})$. Future multidentate phosphine ligand designs in group 6 N_2 systems are aimed at suppressing metal hydride formation by tuning the amine basicity and modifying the location of the amine groups in the second coordination sphere. Further investigations of N_2 reduction to NH_3 with $\mathbf{2}(\mathbf{N_2})$ by the addition of protons and a chemical reductant, and under electrocatalytic conditions, is being examined in our laboratory.

EXPERIMENTAL SECTION

General Experimental Procedures. All synthetic procedures were performed under an atmosphere of N_2 using standard Schlenk or glovebox techniques. Reactions performed with $^{15}N_2$ gas were subsequently handled in the glovebox under an atmosphere of argon. Unless described otherwise, all reagents were purchased from commercial sources and were used as received. Protio solvents were dried by passage through activated alumina columns in an Innovative Technology, Inc., PureSolv solvent purification system and stored under N_2 or argon until use. $^{15}N_2$ (98%) gas and THF-d_8 were purchased from Cambridge Isotope Laboratories. THF-d_8 was dried over NaK and vacuum transferred before use. 1,2-Bis(dimethylphosphino)ethane and bis(dimethylphosphino)methane were purchased from Strem Chemicals Inc. Magnesium powder and triflic acid were purchased from Sigma-Aldrich. $KB(C_6F_5)_4$ was purchased from Boulder Scientific. $H(OEt_2)_2(B(C_6F_5)_4$[40] and *fac*-$[CrCl_3(P^{Ph}{}_3N^{Bn}{}_3)]$[16] ($\mathbf{1}(\mathbf{Cl})_3$) were prepared as previously described. The ^1H, ^{13}C, ^{15}N, and ^{31}P NMR spectra were collected in thin-walled NMR tubes on a Varian Inova or NMRS 500 MHz spectrometer at 25 °C unless otherwise indicated. ^1H and ^{13}C NMR chemical shifts are referenced to residual protio solvent resonances in the deuterated solvent. ^{31}P NMR chemical shifts are proton decoupled unless otherwise noted and referenced to H_3PO_4 as an external reference. ^{15}N NMR chemical shifts were referenced to $CH_3{}^{15}NO_2$ (δ = 0) as an external reference. ^{31}P NMR simulation was generated using *gNMR*.[50] Infrared spectra were recorded on a Thermo Scientific Nicolet iS10 FT-IR spectrometer as a KBr pellet under a purge stream of nitrogen gas. In situ IR experiments were recorded on a Mettler-Toledo ReactIR 15 spectrometer equipped with a liquid nitrogen cooled MCT detector, connected to a 1.5 m AgX Fiber DST series (9.5 mm × 203 mm) probe with a silicon sensor. Experiments were performed in a 5 mL two-neck pear-shaped flask under a dinitrogen atmosphere. IR spectra were collected in intervals of 15 s in the normal collection mode. In situ IR experiments typically used 5 mg of $\mathbf{2}(\mathbf{N_2})$ dissolved in ∼1.0−1.5 mL of THF. Cyclic voltammetry was performed in a Vacuum Atmospheres Nexus II glovebox under an N_2 atmosphere using a CH Instruments model 620D or 660C potentiostat. Measurements were performed using standard three-electrode cell

DOI: 10.1021/acs.inorgchem.5b00351
Inorg. Chem. 2015, 54, 4827−4839

containing a 1 mm PEEK-encased glassy carbon working electrode, Cypress Systems EE040, a 3 mm glassy carbon rod (Alfa) as the counterelectrode, and a silver wire suspended in electrolyte solution and separated from the analyte solution by a Vycor frit (CH Instruments 112) as the pseudoreference electrode in THF with 0.20 M tetrabutylammonium tetrakis(pentafluorophenyl)borate as the supporting electrolyte. Prior to the acquisition of each voltammogram, the working electrode was polished using 0.1 μm γ-alumina (BAS CF-1050), and rinsed with THF. Decamethylferrocene was used as an internal reference, and all potentials are reported versus the ferrocenium/ferrocene couple at 0.0 V. Elemental analysis was performed by Atlantic Microlabs, Norcross, GA.

[Cr(N$_2$)(dmpe)(P^{Ph}$_3$N^{Bn}$_3$)], 2(N$_2$): 1(Cl)$_3$. (0.062 g, 0.070 mmol), dmpe (0.009 g, 0.059 mmol), and Mg powder (0.50 g, 2.0 mmol) was stirred under an N_2 atmosphere in 40 mL of THF for 36 h.[11,12] The red solution was filtered through a syringe filter, and the solvent was removed under a vacuum. The red solids were extracted with Et_2O (3 × 4 mL), and the soluble red product was filtered through a syringe filter and the solvent was removed under vacuum. The red solids were dissolved in pentane and filtered through a syringe filter. Slow evaporation of the pentane solution yielded red crystals that were collected and dried under a vacuum. Yield: 0.055 g, 80%. ^{1}H NMR (500 MHz, THF-d_8, 298 K): δ 7.58−6.98 (30H, PC_6H_5 and $NCH_2C_6H_5$), 3.70 (m, 4H, $NCH_2C_6H_5$), 3.54 (s, 2H, $NCH_2C_6H_5$), 3.47 (m, 2H, NCH_2P), 3.24 (dd, 2H, J_{HH} = 13 Hz, J_{HP} = 3 Hz, NCH_2P), 3.16 (d, 2H, J_{HH} = 13 Hz, NCH_2P), 3.03 (dd, 2H, J_{HH} = 13 Hz, J_{HP} = 3 Hz, NCH_2P), 2.91 (m, 2H, NCH_2P), 2.71 (d, 2H, J_{HH} = 13 Hz, NCH_2P), 1.12 (m, 6H, CH_3P), 0.86 (m, 2H, PCH_2CH_2P), 0.53 (m, 2H, PCH_2CH_2P), 0.24 (m, 6H, CH_3P). ^{13}C{^{1}H} NMR (125 MHz, THF-d_8): δ 126.4−130.0 (PC_6H_5 and $NCH_2C_6H_5$), 67.7 ($NCH_2C_6H_5$), 68.1 ($NCH_2C_6H_5$), 63.15 (NCH_2P), 60.33 (NCH_2P), 31.42 (PCH_2CH_2P), 22.27 (CH_3P), 13.34 (CH_3P). ^{31}P{^{1}H} NMR (202 MHz, THF-d_8): δ 64.5 (m, A/A′ of AA′XX′Y multiplet $J_{AA'}$ = 14 Hz, J_{AX} = 19.3 Hz, $J_{AX'}$ = 7 Hz, J_{AY} = 27.4 Hz, $J_{A'Y}$ = 20 Hz 2P, dmpe), 44.1 (m, X/X′ of AA′XX′Y multiplet $J_{XX'}$ = 7.2 Hz, J_{XY} = 26.5 Hz, $J_{X'Y}$ = 27.3 Hz 2P, P^{Ph}$_3$N^{Bn}$_3$), 38.1 (m, Y of AA′XX′Y multiplet, 1P, P^{Ph}$_3$N^{Bn}$_3$). IR (THF) cm^{-1}: $\nu^{14}{}_{N2}$ 1918 (s), (KBr) 1912 (s). Anal. Calcd for $C_{51}H_{64}CrN_5P_5$: C, 64.21; H, 6.76; N, 7.34. Found: C, 64.58; H, 6.91; N, 7.20.

[Cr(^{15}N$_2$)(dmpe)(P^{Ph}$_3$N^{Bn}$_3$)], 2(^{15}N$_2$): 2(^{15}N$_2$). can be prepared as described above under an atmosphere of $^{15}N_2$ gas, with the reaction workup performed under argon. Alternatively, **2(^{15}N$_2$)** is conveniently generated by rigorously mixing a degassed sample of **2(N$_2$)** in THF under an atmosphere of $^{15}N_2$ gas. ^{15}N{^{1}H} NMR (50 MHz, THF-d_8): δ −10.3 (br, N_p, 1N), −14.5 (d, J_{NN} = 7 Hz, N_d, 1N). IR (THF) cm^{-1}: $\nu^{15}{}_{N2}$ 1855 (s).

[Cr(H)(^{15}N$_2$)(dmpe)(P^{Ph}$_3$N^{Bn}$_3$)], [2(H)(^{15}N$_2$)]$^+$. $[H(OEt_2)_2][B(C_6F_5)_4]$ (0.0047 g, 0.0055 mmol) in 40 μL THF-d_8 was added to a septum capped NMR tube containing **2(^{15}N$_2$)** (0.0053 g, 0.0054 mmol) at −78 °C, resulting in a color change from red to orange. The reaction was quickly mixed and inserted into an NMR probe maintained at −50 °C. ^{1}H NMR (500 MHz, THF-d_8, −50 °C): δ 7.59−7.27 (30H, PC_6H_5 and $NCH_2C_6H_5$), 4.00 (d, 2H, $NCH_2C_6H_5$), 3.80 (m, 4H, $NCH_2C_6H_5$ and NCH_2P), 3.68 (s, 2H, $NCH_2C_6H_5$), 3.36 (m, NCH_2P (overlap with $O(CH_2CH_3)_2$), 3.22 (m, 4H, NCH_2P), 2.83 (d, 2H, NCH_2P), 1.36 (m, 2H, PCH_2CH_2P), 1.27−1.19 (m, 6H, CH_3P), 0.92 (m, 2H, PCH_2CH_2P), 0.08 (m, 6H, CH_3P), −6.26 (sextet, $^2J_{HP}$ = 63 Hz, 1H, Cr-H). ^{31}P{^{1}H} NMR (202 MHz, THF-d_8, −30 °C): δ 62.0 (br, 2P, dmpe), 35.9 (m, 1P, P^{Ph}$_3$N^{Bn}$_3$), 26.8 (br, 2P, P^{Ph}$_3$N^{Bn}$_3$). ^{15}N{^{1}H} NMR (50 MHz, THF-d_8, −50 °C): δ −9.6 (br, N_d, 1N), −28.9 (br, N_p, 1N). IR (THF) cm^{-1}: $\nu(^{14}{}_{N2})$ 2006 (s), ν_{Cr-H} = 1952 (w). This product is thermally sensitive with N_2 loss occurring slowly above −30 °C.

General Procedure for Formation of NH$_3$ from 2(N$_2$). In a typical reaction, ∼10 mg (∼12−15 mmol) of **2(N$_2$)** was dissolved in THF (10 mL) in a 50 mL Schlenk flask. The flask was cooled to −78 °C in a dry ice/acetone bath and triflic acid (20 equiv) was added to the stirring solution resulting in a rapid color change from red-orange to yellow. After stirring vigorously at −78 °C for 21 h, the solution was then stirred at −40 °C for an additional 2 h before being warmed to room temperature. The reaction was frozen, and a solution of KO^{t}Bu (200 equiv) in THF/MeOH (2 mL/8 mL) was added. The reaction was stirred while warming to room temperature and then distilled under a vacuum into a flask containing 4 mL of a 2 M aqueous HCl solution to form NH_4Cl. The reactions were analyzed for NH_3 and N_2H_4 using the indophenol method[51] and *p*-(dimethylamino)-benzaldehyde[52] reagent, respectively.

Theoretical Calculations. All structures were fully optimized without symmetry constraints using the B3P86[53] functional as implemented in Gaussian 09.[54] For the structures with fixed Cr−N−N angles, constrained geometry optimizations were performed for the remaining degrees of freedom. The Stuttgart basis set with effective core potential (ECP)[55] was used for Cr, and the 6-31G* basis sets[56] were used for H, C, N, and P. For hydrogen atoms bound directly to nitrogen or Cr, a polarization function was added (6-31G**). Each stationary point was confirmed by frequency calculation at the same level of theory to be a real minimium (no imaginary frequencies). Gas phase free energies were obtained from zero-point energies, thermal corrections, and entropy terms computed at 1 atm and 223 K. The solvation free energy contribution to the total free energy in THF was calculated using the CPCM model[57] in Gaussian 09 at the same level of theory as that for optimization. Bondi radii were used with a scale factor (α) of 1.0. All calculated pK_a values are for THF solutions and are calculated relative to the value of Et_3NH^+ (pK_a = 12.5),[58] which is assigned as an experimental value to anchor the calculated pK_a scale.

X-ray Diffraction Study. X-ray diffraction data were collected on a Bruker-AXS Kappa APEX II CCD diffractometer with 0.71073 Å Mo−Kα radiation. A selected crystal was mounted using NVH immersion oil onto a nylon fiber and cooled to the data collection temperature of 100 K. Unit cell parameters were obtained from 90 data frames, 0.3° Φ, from three different sections of the Ewald sphere. Cell parameters were retrieved using APEX II software[59] and refined using SAINT+[60] on all observed reflections. Each data set was treated with SADABS[61] absorption corrections based on redundant multiscan data. The structure was solved direct methods and refined by least-squares method on F^2 using the SHELXL program package.[62]

■ ASSOCIATED CONTENT

Supporting Information

Figures, tables, text, and a CIF file including NMR spectral data, crystallographic information, an experimental procedure for the preparation of *trans*-[Cr(^{15}N$_2$)$_2$(dmpe)$_2$], supplementary computational studies, and Cartesian coordinates for computed molecules. This material is available free of charge via the Internet at http://pubs.acs.org.

■ AUTHOR INFORMATION

Corresponding Author

*E-mail: Michael.Mock@pnnl.gov.

Notes

The authors declare no competing financial interest.

■ ACKNOWLEDGMENTS

This work was supported as part of the Center for Molecular Electrocatalysis, an Energy Frontier Research Center funded by the U.S. Department of Energy Office of Science, Office of Basic Energy Sciences. Computational resources were provided by the National Energy Research Scientific Computing Center (NERSC) at Lawrence Berkeley National Laboratory. Pacific Northwest National Laboratory is operated by Battelle for the DOE.

■ REFERENCES

(1) (a) Hoffman, B. M.; Lukoyanov, D.; Yang, Z. Y.; Dean, D. R.; Seefeldt, L. C. *Chem. Rev.* **2014**, *114*, 4041−4062. (b) Hoffman, B. M.; Lukoyanov, D.; Dean, D. R.; Seefeldt, L. C. *Acc. Chem. Res.* **2013**, *46*,

DOI: 10.1021/acs.inorgchem.5b00351
Inorg. Chem. 2015, 54, 4827−4839

587−595. (c) Lukoyanov, D.; Yang, Z.-Y.; Barney, B. M.; Dean, D. R.; Seefeldt, L. C.; Hoffman, B. M. *Proc. Natl. Acad. Sci. U. S. A.* **2012**, *109*, 5583−5587.
(2) (a) Rodriguez, M. M.; Bill, E.; Brennessel, W. W.; Holland, P. L. *Science* **2011**, *334*, 780−783. (b) Erisman, J. W.; Sutton, M. A.; Galloway, J.; Klimont, Z. W. W. *Nat. Geosci.* **2008**, *1*, 636−639.
(3) Chatt, J.; Dilworth, J. R.; Richards, R. L. *Chem. Rev.* **1978**, *78*, 589−625.
(4) Chatt, J.; Pearman, A. J.; Richards, R. L. *Nature* **1975**, *253*, 39−40.
(5) Baumann, J. A.; Bossard, G. E.; George, T. A.; Howell, D. B.; Koczon, L. M.; Lester, R. K.; Noddings, C. M. *Inorg. Chem.* **1985**, *24*, 3568−3578.
(6) George, T. A.; Tisdale, R. C. *J. Am. Chem. Soc.* **1985**, *107*, 5157−5159.
(7) George, T. A.; Ma, L.; Shailh, S. N.; Tisdale, R. C.; Zubieta, J. *Inorg. Chem.* **1990**, *29*, 4789−4796.
(8) George, T. A.; Tisdale, R. C. *Inorg. Chem.* **1988**, *27*, 2909−2912.
(9) Broda, H.; Hinrichsen, S.; Tuczek, F. *Coord. Chem. Rev.* **2013**, *257*, 587−598.
(10) (a) Söncksen, L.; Gradert, C.; Krahmer, J.; Nather, C.; Tuczek, F. *Inorg. Chem.* **2013**, *52*, 6576−6589. (b) Broda, H.; Hinrichsen, S.; Krahmer, J.; Nather, C.; Tuczek, F. *Dalton Trans.* **2014**, *43*, 2007−2012. (c) Broda, H.; Krahmer, J.; Tuczek, F. *Eur. J. Inorg. Chem.* **2014**, *2014*, 3564−3571.
(11) Yandulov, D. V.; Schrock, R. R. *Science* **2003**, *301*, 76−78.
(12) (a) Arashiba, K.; Miyake, Y.; Nishibayashi, Y. *Nat. Chem.* **2011**, *3*, 120−125. (b) Arashiba, K.; Kinoshita, E.; Kuriyama, S.; Eizawa, A.; Nakajima, K.; Tanaka, H.; Yoshizawa, K.; Nishibayashi, Y. *J. Am. Chem. Soc.* **2015**, DOI: 10.1021/jacs.5b02579.
(13) Anderson, J. S.; Rittle, J.; Peters, J. C. *Nature* **2013**, *501*, 84−87.
(14) (a) Vidyaratne, I.; Scott, J.; Gambarotta, S.; Budzelaar, P. H. M. *Inorg. Chem.* **2007**, *46*, 7040−7049. (b) MacKay, B. A.; Fryzuk, M. D. *Chem. Rev.* **2004**, *104*, 385−401.
(15) Mock, M. T.; Chen, S.; Rousseau, R.; O'Hagan, M. J.; Dougherty, W. G.; Kassel, W. S.; DuBois, D. L.; Bullock, R. M. *Chem. Commun.* **2011**, *47*, 12212−12214.
(16) Mock, M. T.; Chen, S.; O'Hagan, M.; Rousseau, R.; Dougherty, W. G.; Kassel, W. S.; Bullock, R. M. *J. Am. Chem. Soc.* **2013**, *135*, 11493−11496.
(17) (a) Girolami, G. S.; Salt, J. E.; Wilkinson, G. *J. Am. Chem. Soc.* **1983**, *105*, 5954−5956. (b) Salt, J. E.; Girolami, G. S.; Wilkinson, G.; Motevalli, M.; Thornton-Pett, M.; Hursthouse, M. B. *J. Chem. Soc., Dalton Trans.* **1985**, 685−692.
(18) Edwards, P. G.; Fleming, J. S.; Sudantha, S. S.; Coles, S. J.; Hursthouse, M. B. *J. Chem. Soc., Dalton Trans.* **1996**, 1801−1807.
(19) Baker, R. J.; Davies, P. C.; Edwards, P. G.; Farley, R. D.; Liyanage, S. S.; Murphy, D. M.; Yong, B. *Eur. J. Inorg. Chem.* **2002**, 1975−1984.
(20) Jones, D. J.; Edwards, P. G.; Tooze, R. P.; Albers, T. *J. Chem. Soc., Dalton Trans.* **1999**, 1045−1046.
(21) Diel, B. N.; Brandt, P. F.; Haltiwanger, R. C.; Hackney, M. L. J.; Norman, A. D. *Inorg. Chem.* **1989**, *28*, 2811−2816.
(22) Tuczek, F.; Horn, K. H.; Lehnert, N. *Coord. Chem. Rev.* **2003**, *245*, 107−120.
(23) Gradert, C.; Stucke, N.; Krahmer, J.; Näther, C.; Tuczek, F. *Chem.—Eur. J.* **2014**, *21*, 1130−1137.
(24) Karsch, H. H. *Angew. Chem., Int. Ed.* **1977**, *16*, 56−57.
(25) Cugny, J.; Schmalle, H. W.; Fox, T.; Blacque, O.; Alfonso, M.; Berke, H. *Eur. J. Inorg. Chem.* **2006**, 540−552.
(26) Hussain, W.; Leigh, G. J.; Ali, H. M.; Pickett, C. J.; Rankin, D. A. *J. Chem. Soc., Dalton Trans.* **1984**, 1703−1708.
(27) Donavon-Mtunzi, S.; Richards, R. L.; Mason, J. *J. Chem. Soc., Dalton Trans.* **1984**, 469−474.
(28) Krahmer, J.; Broda, H.; Näther, C.; Peters, G.; Thimm, W.; Tuczek, F. *Eur. J. Inorg. Chem.* **2011**, 4377−4386.
(29) Klatt, K.; Stephan, G.; Peters, G.; Tuczek, F. *Inorg. Chem.* **2008**, *47*, 6541−6550.
(30) Stephan, G. C.; Peters, G.; Lehnert, N.; Habeck, C. M.; Näther, C.; Tuczek, F. *Can. J. Chem.* **2005**, *83*, 385−402.
(31) Carmona, E.; Marin, J. M.; Poveda, M. L.; Atwood, J. L.; Rogers, R. D. *J. Am. Chem. Soc.* **1983**, *105*, 3014−3022.
(32) Galindo, A.; Gutierrez, E.; Monge, A.; Paneque, M.; Pastor, A.; Perez, P. J.; Rogers, R. D.; Carmona, E. *J. Chem. Soc., Dalton Trans.* **1995**, 3801−3808.
(33) Dadkhah, H.; Dilworth, J. R.; Fairman, K.; Kan, C. T.; Richards, R. L. *J. Chem. Soc., Dalton Trans.* **1985**, 1523−1526.
(34) Chatt, J.; Pearman, A. J.; Richards, R. L. *J. Chem. Soc., Dalton Trans.* **1977**, 2139−2142.
(35) Weiss, C. J.; Groves, A. N.; Mock, M. T.; Dougherty, W. G.; Kassel, W. S.; Helm, M. L.; DuBois, D. L.; Bullock, R. M. *Dalton Trans.* **2012**, *41*, 4517−4529.
(36) Hu, C.; Hodgeman, W. C.; Bennett, D. W. *Inorg. Chem.* **1996**, *35*, 1621−1626.
(37) Carmona, E.; Galindo, A.; Poveda, M. L.; Rodgers, R. D. *Inorg. Chem.* **1985**, *24*, 4033−4039.
(38) Sobota, P.; Jezowska-Trzebiatowska, B. *J. Organomet. Chem.* **1977**, *131*, 341−345.
(39) (a) Stephan, G. C.; Näther, C.; Sivasankar, C.; Tuczek, F. *Inorg. Chim. Acta* **2008**, *361*, 1008−1019. (b) Stephan, G.; Nather, C.; Tuczek, F. *Acta Crystallogr., Sect. E: Struct. Rep. Online* **2008**, *64*, m629.
(40) Heiden, Z. M.; Chen, S.; Mock, M. T.; Dougherty, W. G.; Kassel, W. S.; Rousseau, R.; Bullock, R. M. *Inorg. Chem.* **2013**, *52*, 4026−4039.
(41) Oztopcu, O.; Holzhacker, C.; Puchberger, M.; Weil, M.; Mereiter, K.; Veiros, L. F.; Kirchner, K. *Organometallics* **2013**, *32*, 3042−3052.
(42) Hoffmann, R.; Beier, B. F.; Muetterties, E.; Rossi, A. R. *Inorg. Chem.* **1977**, *16*, 511−522.
(43) (a) Datta, S.; Dezube, B.; Kouba, J. K.; Wreford, S. S. *J. Am. Chem. Soc.* **1978**, *100*, 4404−4412. (b) Bond, A. M.; Colton, R.; Jakowski, J. J. *Inorg. Chem.* **1975**, *14*, 2526−2530.
(44) Weiss, C. J.; Egbert, J. D.; Chen, S.; Helm, M. L.; Bullock, R. M.; Mock, M. T. *Organometallics* **2014**, *33*, 2189−2200.
(45) Labios, L. A.; Weiss, C. J.; Egbert, J. D.; Lense, S.; Bullock, R. M.; Dougherty, W. G.; Kassel, W. S.; Mock, M. T. *Z. Anorg. Allg. Chem.* **2015**, *641*, 105−117.
(46) In this work, the geometry of triethylamine (the anchor for the computed pK_a values) was optimized to a more stable configuration (ΔE = −2.7 kcal/mol). As a result, the computed pK_a values for the P_4N_4 system are slightly larger than those reported previously.
(47) The geometry of a singlet diazene intermediate $[\mathbf{2(NHNH)'}]^{2+}$ was unstable during optimization (the proton on the proximal nitrogen transfers to the Cr center) and was not given further consideration in this report.
(48) Wiberg, N.; Bachhuber, H.; Fischer, G. *Angew. Chem., Int. Ed.* **1972**, *11*, 829−830.
(49) A more detailed investigation of the dependence of $^2[\mathbf{2(NNH_2)'}]^+$ on the identity of the supporting ligand is beyond the scope of this report, but it is worth noting that when phosphine (PH_3) is added as a ligand to the vacant axial position of the hydrazido intermediate in the P_4N_4 system (in order to mimic the P5 coordination environment in the P_3N_3 system), the structure of the Cr-N-N unit upon geometry optimization was similar to that found in the P_3N_3 system.
(50) Budzelaar, P. H. M. *gNMR 5.0*; IvorySoft, 1995−2006.
(51) (a) Chaney, A. L.; Marbach, E. P. *Clin. Chem.* **1962**, *8*, 130−132. (b) Weatherburn, M. W. *Anal. Chem.* **1967**, *39*, 971−974.
(52) Watt, G. W.; Chrisp, J. D. *Anal. Chem.* **1952**, *24*, 2006−2008.
(53) (a) Becke, A. D. *J. Chem. Phys.* **1993**, *98*, 5648−5652. (b) Perdew, J. P. *Phys. Rev. B* **1986**, *33*, 8822−8824.
(54) Frisch, M. J.; G, W. T., Schlegel, H. B.; Scuseria, G. E.; Robb, M. A.; Cheeseman, J. R.; Scalmani, G.; Barone, V.; Mennucci, B.; Petersson, G. A.; Nakatsuji, H.; Caricato, M.; Li, X.; Hratchian, H. P.; Izmaylov, A. F.; Bloino, J.; Zheng, G.; Sonnenberg, J. L.; Hada, M.; Ehara, M.; Toyota, K.; Fukuda, R.; Hasegawa, J.; Ishida, M.; Nakajima, T.; Honda, Y.; Kitao, O.; Nakai, H.; Vreven, T.; Montgomery, J. A.Jr.;

DOI: 10.1021/acs.inorgchem.5b00351
Inorg. Chem. 2015, 54, 4827−4839

Peralta, J. E.; Ogliaro, F.; Bearpark, M.; Heyd, J. J.; Brothers, E.; Kudin, K. N.; Staroverov, V. N.; Kobayashi, R.; Normand, J.; Raghavachari, K.; Rendell, A.; Burant, J. C.; Iyengar, S. S.; Tomasi, J.; Cossi, M.; Rega, N.; Millam, J. M.; Klene, M.; Knox, J. E.; Cross, J. B.; Bakken, V.; Adamo, C.; Jaramillo, J.; Gomperts, R.; Stratmann, R. E.; Yazyev, O.; Austin, A. J.; Cammi, R.; Pomelli, C.; Ochterski, J. W.; Martin, R. L.; Morokuma, K.; Zakrzewski, V. G.; Voth, G. A.; Salvador, P.; Dannenberg, J. J.; Dapprich, S.; Daniels, A. D.; Farkas, O.; Foresman, J. B.; Ortiz, J. V.; Cioslowski, J.; Fox, D. J. *Gaussian 09, Revision A.01*; Gaussian, Inc.: Wallingford, CT, 2009.

(55) Andrae, D.; Häußermann, U.; Dolg, M.; Stoll, H.; Preuß, H. *Theor. Chem. Acc.* **1990**, *77*, 123−141.

(56) (a) Francl, M. M.; Pietro, W. J.; Hehre, W. J.; Binkley, J. S.; Gordon, M. S.; DeFrees, D. J.; Pople, J. A. *J. Chem. Phys.* **1982**, *77*, 3654−3665. (b) Rassolov, V. A.; Ratner, M. A.; Pople, J. A.; Redfern, P. C.; Curtiss, L. A. *J. Comput. Chem.* **2001**, *22*, 976−984.

(57) Barone, V.; Cossi, M. *J. Phys. Chem. A* **1998**, *102*, 1995−2001.

(58) (a) Abdur-Rashid, K.; Fong, T. P.; Greaves, B.; Gusev, D. G.; Hinman, J. G.; Landau, S. E.; Lough, A. J.; Morris, R. H. *J. Am. Chem. Soc.* **2000**, *122*, 9155−9171. (b) Rodima, T.; Kaljurand, I.; Pihl, A.; Maemets, V.; Leito, I.; Koppel, I. *J. Org. Chem.* **2002**, *67*, 1873−1881.

(59) *APEX II, v. 2009.3*; Bruker AXS: Madison, WI, 2009.

(60) *SAINT+, v. 7.56A*; Bruker AXS: Madison, WI, 2009.

(61) *SADABS, v. 2008/1*; Bruker AXS Inc.: Madison, WI, 2008.

(62) Sheldrick, G. M.; *SHELXTL, v. 2008*; Bruker AXS Inc.: Madison, WI, 2008.

DOI: 10.1021/acs.inorgchem.5b00351
Inorg. Chem. 2015, 54, 4827−4839